

# Influence of lanthanum on the microstructure, mechanical property and corrosion resistance of magnesium alloy

Yu Fan · Guohua Wu · Hongtao Gao ·  
Guanqun Li · Chunquan Zhai

Received: 2 March 2005 / Accepted: 14 October 2005 / Published online: 8 June 2006  
© Springer Science+Business Media, LLC 2006

**Abstract** The microstructure, mechanical property and corrosion behavior of AZ91D with addition of lanthanum were investigated. With adding 1% lanthanum, the ultimate tensile strength and the elongation increased by 21.1% and by 101.2%, respectively. This mainly caused by the refinement of the  $\beta$  phase and the formation of  $Al_{11}La_3$  strengthening phase. With adding 1% lanthanum in AZ91D alloy, the weight loss corrosion rate decreased to 47.2%. But when lanthanum content is over 1%, the corrosion rate increased. Small amount of lanthanum could form the small  $\beta$  phase similar to reticular structure, which could restrain the corrosion at some extent; large amount of lanthanum caused the depletion of aluminum in  $\alpha$  matrix, which increased the corrosion rate.

## Introduction

Magnesium alloys have a high strength-to-weight ratio, and thus appear to be promising alternatives to aluminum and steel alloys used in the automotive industry. Although a wide variety of applications can be envisaged for magnesium alloys, the use at present is limited mainly due to inferior corrosion property [1–5]. And magnesium alloy with Al and Zn have found wide spread application in the automobile sector. Corrosion performance is, therefore, quite important as it concerns the operating life of magnesium alloy components in a vehicle.

The addition of rare earth is an effective way to improve the mechanical properties of magnesium alloys, and the corrosion resistance in some degree. Some works have been reported [6–9] on the corrosion behavior of the commercial alloy AZ91, which is widely used in low-temperature applications. Nevertheless, there are a few works concerning the effect of rare earth additions on the corrosion performance [10–12] and no works concerning the effect of lanthanum on the corrosion performance of magnesium alloys. The aim of the present work was to investigate the influence of lanthanum on the microstructure, mechanical properties and corrosion resistance of magnesium alloys.

## Experimental methods

In this work, four new AZ91D alloys with different lanthanum content were studied and were named as AZL alloys. These alloys were prepared starting with AZ91D and pure lanthanum. The composition of AZ91D determined by ICP-AES is listed in Table 1. AZ91D ingots were melted in an aluminum oxide crucible at 730 °C. Appropriate amounts of lanthanum (99.9% purity) were added into the molten AZ91D alloy. The above procedures were conducted under a flowing protective gas of  $SF_6$  (1 vol.%) and  $CO_2$  (bal.) to prevent burning and oxidation. The melt was held at  $720 \pm 5$  °C for 30 min, and then poured into one permanent mold [13] and one cylindrical metal mold of  $\Phi 45$  mm  $\times$  100 mm. The actual lanthanum content of AZL alloys determined by ICP-AES is listed in Table 2.

Tensile specimens with a gauge section of 15 mm  $\times$  3.5 mm  $\times$  2 mm were cut by electric spark machining from the bottom of the ingots. And other specimens were cut from the cylindrical ingots. Tensile

Y. Fan (✉) · G. Wu · H. Gao · G. Li · C. Zhai  
State Key Laboratory of Metal Matrix Composite, Shanghai  
Jiaotong University, Shanghai 200030, P. R. China  
e-mail: fyspy@sjtu.edu.cn

**Table 1** Chemical compositions of AZ91D alloy (wt.%)

Alloy	Al	Zn	Mn	Fe	Ni	Cu	Mg
AZ91D	8.99	0.709	0.194	0.01	<0.002	<0.002	Bal.

**Table 2** Chemical compositions of the AZL alloys (wt.%)

Alloy	Al	Zn	La	Mg
AZL05	8.99	0.709	0.527	Bal.
AZL1	8.99	0.709	1.064	Bal.
AZL15	8.99	0.709	1.489	Bal.
AZL2	8.99	0.709	1.953	Bal.

tests were conducted on the Zwick T1-FR020TN.A50 electronic universal material testing machine. The Rigaku Dmax-rc X-ray diffractometer and PHILIPS SEM 515 were employed to analyze phase compositions and the corrosion morphology.

The specimens for immersion test were  $\Phi 35$  mm  $\times$  4 mm in size. Then the coupon specimens were polished with 800 grit SiC paper. The specimens were initially cleaned with acetone and distilled water. After immersion tests, the corroded specimens were cleaned with distilled water and dried. They were then immersed in a chromate acid (180 g/L  $\text{CrO}_3$  + 1%  $\text{AgNO}_3$ ) at boiling condition for 3 min to remove the corrosion products. The extent of corrosion was given in weight loss per surface area and time ( $\text{mg cm}^{-2} \text{d}^{-1}$ , MCD).

The specimens for AC and DC electrochemical measurements were 10 mm  $\times$  10 mm  $\times$  4 mm in size, and were polished with 800 grit SiC paper. Then they were welded with electrical wire and embedded in epoxy resin as working electrodes for electrochemical measurements. The exposed area was about 1  $\text{cm}^2$ .

Polarization curves and electrochemical impedance spectra of the specimens were measured in an electrolytic cell containing about 300 mL of 5 wt.% NaCl solution saturated with  $\text{Mg}(\text{OH})_2$  using a Solatron 1,287 + 1,260 electrochemical measurement system. The polarization started from a cathodic potential of about  $-200$  mV relative to the corrosion potential and stopped at an anodic potential 60 mV positive to the corrosion potential. The scanning rate was 0.1667 mV/s.

AC impedance measurements were conducted at the corrosion potentials of the electrodes. The amplitude of applied AC signal was 5 mV, and the measured frequency range was from 1 kHz to 10 mHz.

During the polarization and AC impedance measurements, a three electrode electrochemical cell was used, with a saturated calomel electrode as reference, a platinum counter electrode and a working electrode.

## Experimental results

### Microstructure

In the as-cast condition the microstructure of AZ91D magnesium alloys consists of primary  $\alpha$  grains with the grain boundaries precipitated with large  $\beta$  phase particles [14, 15], shown as Fig. 1a. With the addition of lanthanum, the  $\text{Mg}_{17}\text{Al}_{12}$  phases were gradually refined and some small  $\text{Mg}_{17}\text{Al}_{12}$  precipitates formed. The  $\beta$  precipitate phase appears in two morphologies: large particles and fine lamellar plates, shown as Fig. 2a, c. As shown in Fig. 1 a and b, the addition of lanthanum refined the  $\beta$  phase and formed the reticular  $\beta$  phase on grain boundary.

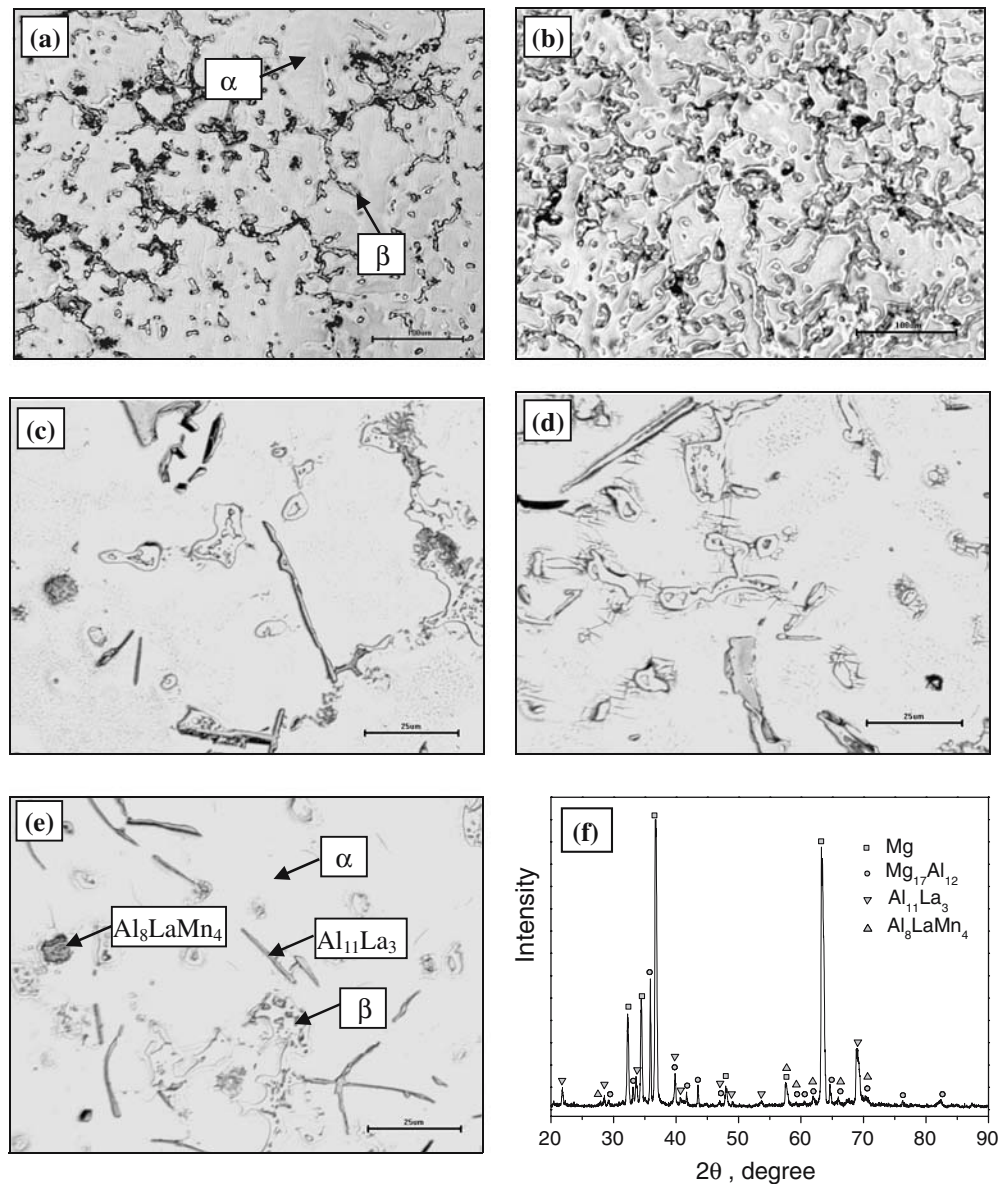
With the addition of lanthanum, some rod-like intermetallic phases are observed in the Fig. 1c–e. By analyzing the SEM (Fig. 2a) and EDAX result (Fig. 2b), it was found that the rod-like phase was Al–La phase. In addition to rod-like Al–La phase, some blocky phases are observed in the Fig. 1 c, e. The results of SEM (Fig. 2c) and EDAX results (Fig. 2d) indicated that the blocky phase was Al–La–Mn ternary phase. In the AZL2 alloy, there are four phases: primary  $\alpha$ ,  $\beta$  phase ( $\text{Mg}_{17}\text{Al}_{12}$ ),  $\text{Al}_{11}\text{La}_3$  and  $\text{Al}_8\text{LaMn}_4$ , shown as Fig. 1 f. By analyzing the XRD of AZL2, it was found that the rod-like Al–La phase was  $\text{Al}_{11}\text{La}_3$ , which was called  $\text{Al}_4\text{La}$  by some researchers, and the block Al–La–Mn phase was  $\text{Al}_8\text{LaMn}_4$ . With increasing lanthanum content, the amount of the rod-like  $\text{Al}_{11}\text{La}_3$  phase increased and its size coarsened. Furthermore, the matrix becomes depleted of aluminum due to the formation of more  $\text{Al}_{11}\text{La}_3$  phase, shown as Fig. 3.

### Mechanical property

The effect of lanthanum on mechanical properties of AZ91D at ambient temperature is shown in Fig. 4. With the increasing of lanthanum addition, the ultimate tensile strength and the elongation both sharply increased. With adding 1% lanthanum, the ultimate tensile strength and the elongation of AZL1 alloy increased by 21.1% and by 101.2%, respectively. When the lanthanum content was more than 1%, the ultimate tensile strength and the elongation of AZL alloys increased slowly. The ultimate tensile strength and the elongation of AZL2 alloy increased to 178.02 MPa and 3.85%, respectively. In addition, the addition of lanthanum had small effect on the yield strength of AZ91D alloys. The yield strength of AZL1 alloy increased by 2.0% compared to that of AZ91D.

The reason of the mechanical property improvement is that the addition of lanthanum not only formed  $\text{Al}_{11}\text{La}_3$  strengthening phase, but also refined  $\beta$  phase. So the addition of lanthanum could improve the mechanical properties of AZ91D magnesium alloy.

**Fig. 1** Optical microstructure of as-cast AZL alloys and XRD of AZL2 alloy: (a) AZ91D, (b) AZL05, (c) AZL1, (d) AZL15, (e) AZL2, (f) XRD of the AZL2 alloy



### Immersion test

Figure 5 shows the effect of lanthanum on the corrosion resistance of AZ91D under immersion conditions (5 wt.% NaCl solution). Firstly, with the increase of lanthanum content, the corrosion rate of AZL alloys decreased obviously. Especially with adding 1% lanthanum, the corrosion rate of AZ91D decreased to  $0.067 \text{ mg cm}^{-2} \text{ d}^{-1}$ , which was about 47.2% of the AZ91D corrosion rate. The addition of lanthanum refined  $\beta$  phase and formed small lamellar  $\beta$  phase, which had a similar to reticular structure. This similar to reticular structure could obviously restrain the corrosion process.

However, when lanthanum content was more than 1%, the corrosion rate sharply increased. With 2% lanthanum addition, the corrosion rate of AZL2 alloy increased by

about 69.0%. The addition of lanthanum refined  $\beta$  phase, but more addition of lanthanum consumed more aluminum by the formation of  $\text{Al}_{11}\text{La}_3$ . So  $\alpha$  matrix was depleted of aluminum, which caused the large increase of corrosion rate of AZ91D alloy.

### Potentiodynamic polarization

The polarization behaviors of AZ91D and the AZL alloys in 5 wt.% NaCl saturated with  $\text{Mg}(\text{OH})_2$  are shown in Fig. 6. As a first remark we noted that the shape of the polarization curves was almost the same for all studied alloys and no passive behavior could be observed during the course of anodic polarization. And this is not consistent with Mathieu's experiment result [16], in which they have found a plateau extending on a large anodic

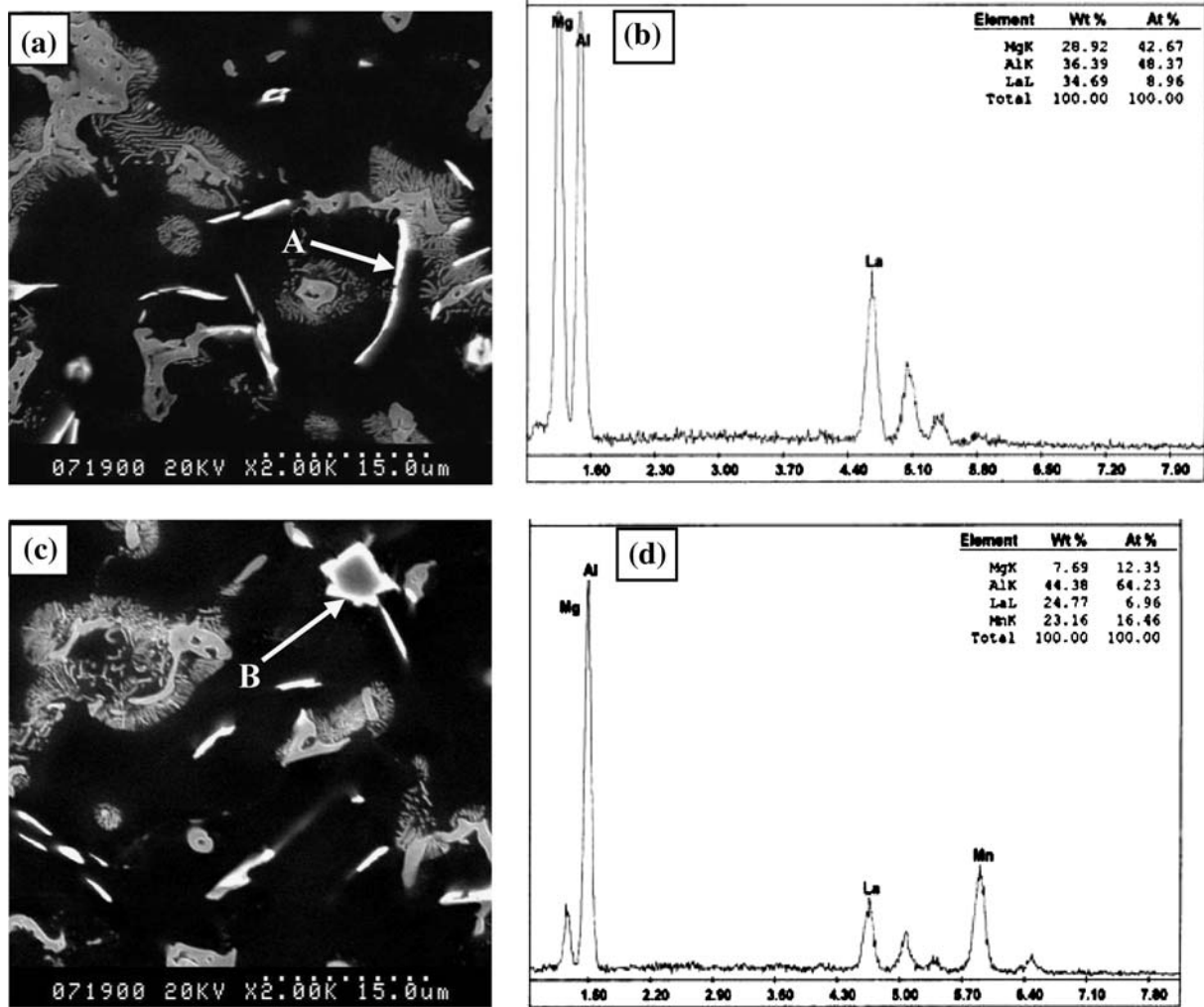


**Fig. 2** (a) Scanning electron micrograph of AZL1; (b) EDAX of the “A” phase (c) Scanning electron micrograph of AZL2; (d) EDAX of the “B” phase

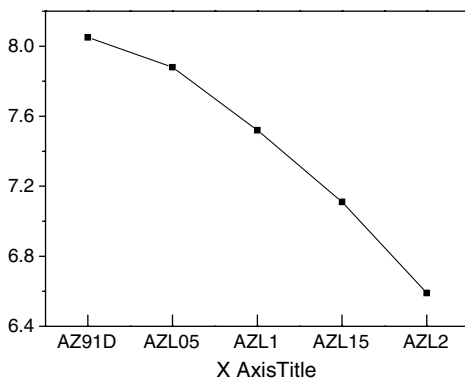


**Fig. 3** Al concentration of AZL alloy in primary Mg

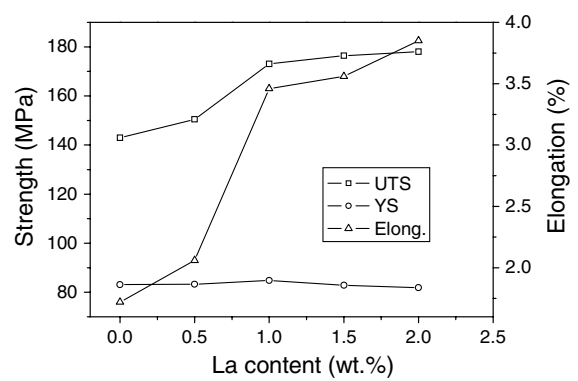


**Fig. 4** Mechanical properties of AZL alloys at room temperature

potential domain ( $I_{corr}$  is about  $10^{-5} A/cm^2$ ) on the polarization curves for the high pressure die-cast and SSP AZ91D magnesium alloy in ASTM D1384 water saturated with  $Mg(OH)_2$ . This is due to the aggressive environment of NaCl solution for magnesium alloys. The

absorption of chloride ions to magnesium surface, transforms  $Mg(OH)_2$  to easily soluble  $MgCl_2$  [17]. So in 5 wt.% NaCl solution saturated with  $Mg(OH)_2$ , there is no passive behavior for potentiodynamic polarization of the AZL alloys.

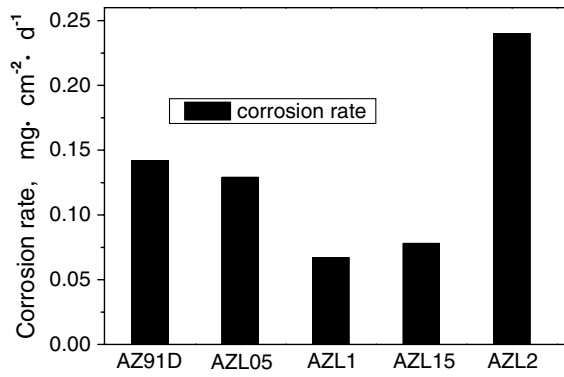


**Fig. 5** Weight loss corrosion rate of the AZL alloys after immersion in 5 wt.% NaCl solution for 3d

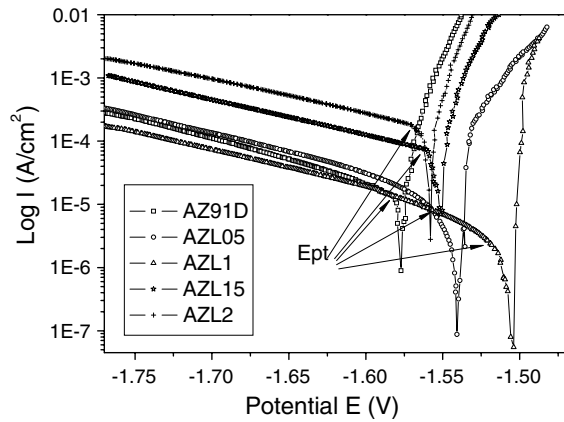


**Fig. 6** Polarization curves of the AZL alloys in 5 wt.% NaCl saturated with Mg(OH)<sub>2</sub>

Another apparent change in the polarization curves of the AZ91D and AZL alloys (Fig. 6) is to shift the polarization curves to more positive potentials. In fact, the shifts result from the different “pitting” potentials (E<sub>pt</sub>) of these alloys. It has been demonstrated that [18] Mg–Al–Zn alloys normally start localized corrosion (pitting) at a potential slightly more negative than their corrosion potentials in a salt solution. On a polarization curve obtained by the potentiodynamic method, and starting potential scanning from a cathodic potential, the “pitting” potential E<sub>pt</sub> is usually indicated by a sudden drop in cathodic current which is immediately followed by anodic current around the corrosion potential. At the “pitting” potential, the initiation of localized corrosion is accompanied by dramatic visible hydrogen evolution from the corroding sites on the electrode surface during polarization curve measurement.

In Fig. 6, the E<sub>pt</sub> is marked on each polarization curve. The E<sub>pt</sub> is an important electrochemical parameter. It indicates the tendency to localized corrosion. A more positive E<sub>pt</sub> means less likely localized corrosion. The dependence of E<sub>pt</sub> on lanthanum content in AZL

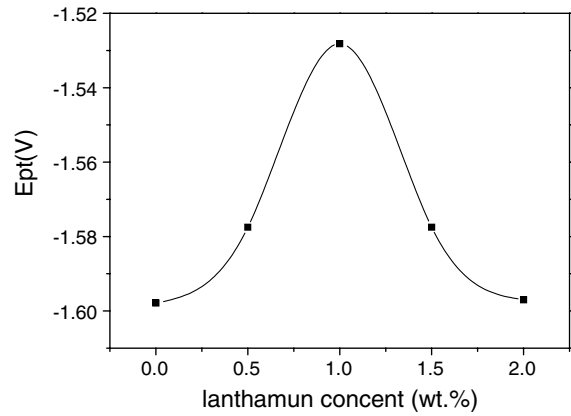


**Fig. 7** Dependence of “pitting” potential (E<sub>pt</sub>) on lanthanum content in the AZL alloys

magnesium alloys is shown in Fig. 7. With 1% lanthanum content, the AZL1 alloy had more positive E<sub>pt</sub>, which was 66 mV higher than the AZ91D E<sub>pt</sub>. This means that the AZL1 alloy is more stable than the AZ91D alloy, which is consistent with the weight loss corrosion rate results (Fig. 5). But with more addition of lanthanum, the formation of more Al<sub>11</sub>La<sub>3</sub> phase caused the depletion of aluminum content in α matrix, which led to the shift of E<sub>pt</sub> to a more negative potential.

The corrosion potential (E<sub>corr</sub>) and the corrosion current density (I<sub>corr</sub>) derived from the polarization are plotted as a function of lanthanum content in Fig. 8. Firstly, the corrosion potential sharply increased with the increase of the lanthanum content. When the lanthanum content reached 1%, the corrosion potential reached the maximum value, which was higher 65.6 mV than the corrosion potential of AZ91D alloy. However, when the lanthanum content was more than 1%, the corrosion potential of AZL alloys decreased with the increase of lanthanum content. Thereafter, with increasing the lanthanum content, the corrosion current density firstly decreased, and then increased, which was consistent with the weight loss results (Fig. 5).

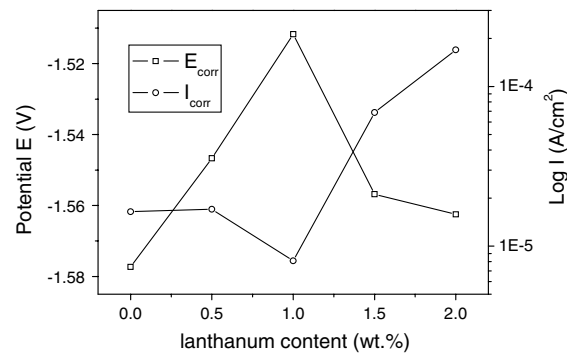


**Fig. 8** Corrosion potential and corrosion current density of the AZL alloys

## Electrochemical impedance spectroscopy

Corrosion damage results from electrochemical reactions, so electrochemical measurements can often reveal the corrosion mechanism. A corroding metal is approximately modeled as a simple electrochemical system consisting of a double-layer capacitance, a solution resistance and a charge transfer resistance. The corrosion mechanism of magnesium sometimes can be estimated through analyzing the measured electrochemical impedance spectrum [18, 19].

In this study, the EIS results of AZ91D and AZL magnesium alloys are presented in Fig. 9. All the alloys have a capacitive semicircle in the high frequency region. Their EIS spectra are similar except for the difference in the diameters of the loops. This means that the corrosion mechanisms of AZL magnesium alloys are the same, but their corrosion rate could be different. The diameter of the capacitive semicircle of a measured Nyquist spectrum is closely related to the corrosion rate. Makar et al. [20] compared corrosion rates calculated from the first capacitive semicircle in the high frequency region with weight loss results for various magnesium alloys, and found that most of the EIS results matched very well with the weight loss data.

With the increase of lanthanum content, the diameter of the first capacitive semicircles firstly increased. After the diameter of AZ91D with 1% lanthanum content increases to maximum, the diameter sharply decreased. Especially the diameter of AZL2 decreased to minimum, which was obviously smaller than the diameter of AZ91D. So if the first capacitive semicircles are taken as the impedance representing the corrosion resistance, the corrosion resistance of AZL alloys firstly increases then decreases as the lanthanum content increases. And this is consistent with the weight loss corrosion results.

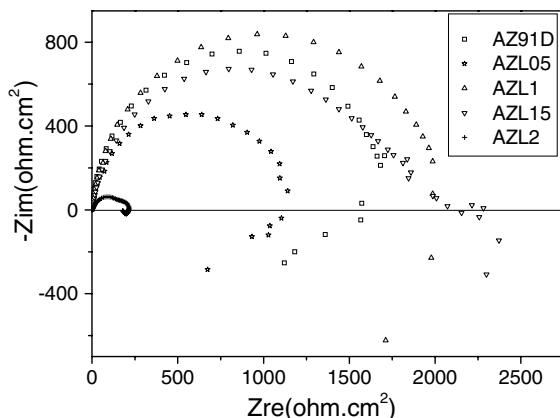


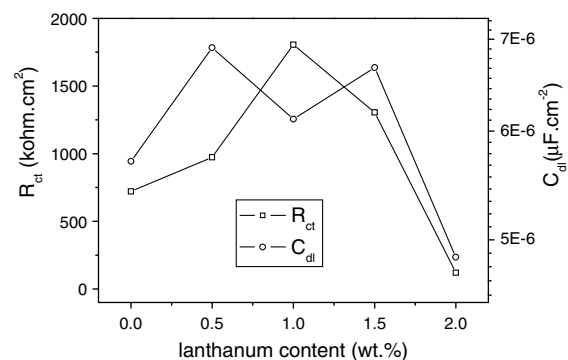
**Fig. 9** Electrochemical impedance spectra of the AZL alloys in 5 wt.% NaCl saturated with  $Mg(OH)_2$

The Nyquist plots of AZL alloys (Fig. 9) have a capacitive semicircle in the high and intermediate frequency region and an inductive semicircle in the low frequency region. The high frequency capacitive semicircle can be attributed to the charge transfer reaction. Thus, for the high frequency capacitive semicircle, a charge transfer resistor  $R_{ct}$  and a capacitor  $C_{dl}$  in parallel can model the electrode/electrolyte interface. A partial data fitting made with Boukamp circuit equivalent software [21] for the charge transfer process produced the charge transfer resistance ( $R_{ct}$ ) and double-layer capacitance ( $C_{dl}$ ). Fig. 10 shows the dependence of the  $R_{ct}$  and  $C_{dl}$  on the lanthanum content of the AZL alloys. The  $R_{ct}$  values correspond to the diameter of the high frequency capacitive semicircle. And the  $R_{ct}$  also corresponds to the polarization resistance ( $R_p$ ) in those cases where the impedance spectrum collapses to RC-R behavior ( $R_{ct} = R_p$ ). In addition,  $1/R_p$  value is proportional to the corrosion rate [22]. So with the increase of lanthanum content, the  $R_{ct}$  value of the AZL alloy firstly increased, and then decreased when the lanthanum content was more than 1%, i.e., the corrosion resistance of the AZL alloys was improved firstly, and then reduced.

Considering the  $C_{dl}$  values, the low value of  $C_{dl}$  for the magnesium alloy implies the formation of a relatively thick and compact protective film on the metal surface [23]. In this study, the increase of the  $R_{ct}$  is not accompanied by a breakdown of the  $C_{dl}$  values, even the  $C_{dl}$  values are increased with the increase of the  $R_{ct}$ . This shows that the AZL alloys could not form an effective protective film in 5 wt.% NaCl solution saturated with  $Mg(OH)_2$  due to the aggressive environment of NaCl solution for magnesium alloys.

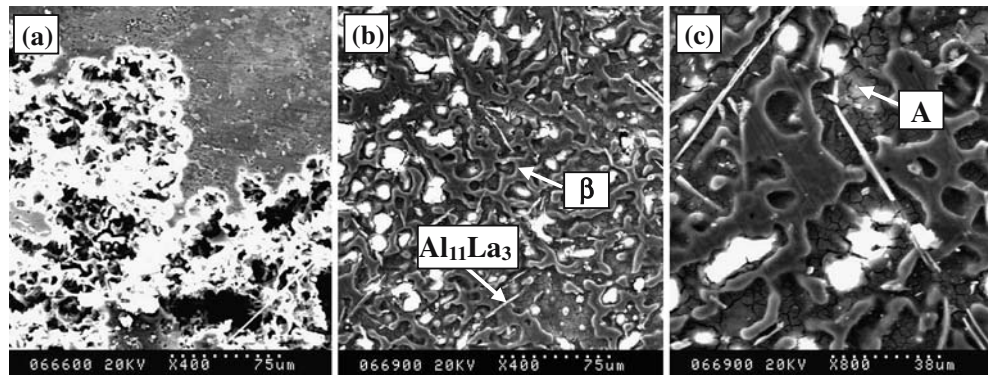
## Corrosion morphology

Figure 11 was taken on immersion test specimens after removed the corrosion products. In the case of as-cast AZ91D, corrosion mainly occurred in the interior of a



**Fig. 10** Charge transfer resistance ( $R_{ct}$ ) and double-layer capacity ( $C_{dl}$ ) of the AZL alloys

**Fig. 11** SEM of corrosion morphology on AZL alloys (a) AZ91D, (b) AZL1, (c) AZL1



grain, and developed from grain to grain. The corroded matrix exhibits a porous morphology, shown as Fig. 11a. It was obvious that many deep pits formed in the corroded areas on AZ91D during the immersion corrosion test and the corrosion was localized.

However, the depth of the corroded areas on AZL alloy (Fig. 11b) was relatively shallow and uniform compared to the corrosion morphology of AZ91D. The morphology observed on the corroded areas of AZL1 was similar to the reticular  $\beta$  phase on grain boundary (Fig. 1b). This indicated the adding of lanthanum promoted the forming of more continuous  $\beta$  phase on grain boundary, which acted as a corrosion barrier [24]. And this result was consistent with the corrosion rate of immersion tests. As shown in Fig. 11c area ‘‘A’’, the corrosion film, which formed after the matrix in the interior of grain has corroded away, has impeded corrosion to some extent.

## Discussions

In the as-cast condition, adding lanthanum into AZ91D magnesium alloy refined the  $\beta$  phase-Mg<sub>17</sub>Al<sub>12</sub> and formed rod-like Al<sub>11</sub>La<sub>3</sub> phase. The precipitation of Al<sub>11</sub>La<sub>3</sub> phase impedes the formation and incipient development of the cracks, which improved the tensile strength [25]. Furthermore, coarse  $\beta$  phase on grain boundary is harmful to the mechanical properties, so the adding of lanthanum could improve the mechanical properties by refined  $\beta$  phase. The rod-like phase-Al<sub>11</sub>La<sub>3</sub> was strengthening phase and small compared to  $\beta$  phase, so it did not promote brittleness.

The secondary phase in a magnesium alloys is normally inert and stable in corrosion. For example, in AZ alloys,  $\beta$  phase is very corrosion resistant and normally not corroded if exposed to a NaCl solution. It was found that lanthanum not only refined  $\beta$  phase, but also formed more continuous and  $\beta$  phase along the grain boundaries in AZ91D alloy. And the reticular  $\beta$  phase effectively confined the development of corrosion from grain to grain and hence significantly reduced the corrosion rate of the alloy [24].

## Conclusion

- (1) The addition of lanthanum refined  $\beta$  phase and formed Al<sub>11</sub>La<sub>3</sub> strengthening phase, which greatly improved the mechanical properties of AZ91D alloy. With adding 1% lanthanum, the ultimate tensile strength and the elongation increased by 21.1% and by 101.2%, respectively.
- (2) The weight loss corrosion rate of AZ91D alloy decreased by adding small amount of lanthanum. With the addition of 1% lanthanum, the corrosion rate decreased to 0.067 mg cm<sup>-2</sup> d<sup>-1</sup>, which was about 47.2% of AZ91D corrosion rate. By adding lanthanum, the formation of similar to reticular structure- $\beta$  phase could restrain the corrosion process. But adding more lanthanum, the corrosion rate of AZ91D alloy increased.
- (3) With increasing lanthanum content, the corrosion potential, the ‘‘pitting’’ corrosion potential (E<sub>pt</sub>) and the charge transfer resistance (R<sub>ct</sub>) all firstly increased, then declined, which was consistent with the weight loss corrosion results.
- (4) So adding 1% lanthanum in AZ91D alloy could improve not only the mechanical properties, but also the corrosion resistance.

**Acknowledgement** The present study is funded by the National High Technology R&D Program of China and National Natural Science Foundation of China (Contract No. 50474005).

## References

1. Rajagopalan B, Mohanty PS, Mallick PK (2004) *Magnesium Technology*:131
2. Baghni M, Yinshun W, Jiuqing L, Wei Z (2004) *Trans Nonferrous Met Soc China* 14:1
3. Song GL, Atrens A, Stjohn D, Nairn J, Li Y (1997) *Corros Sci* 39:855
4. Popov I, Starosvetsky D, Shechtman D (2000) *J Mater Sci* 35:1
5. Nordlien JH, Ono S, Masuko N, Nisancioglu K (1997) *Corros Sci* 39:1397
6. Aung NN, Zhou W (2002) *J Appl Electrochem* 32:1397

7. Mathieu S, Rapin C, Steinmerz J, Steinmetz P (2003) *Corros Sci* 45:2741
8. Ambat R, Aung NN, Zhou W (2000) *Corros Sci* 42:1433
9. Jinko Y, Yim CD, Lim JD (2003) *Mater Sci Forum* 419–422:851
10. Morales ED, Ghali E, Hort N, Dietzel W, Kainer KU (2003) *Mater Sci Forum* 419–422:867
11. Song GL, StJohn D (2002) *J Light Metals* 2:1
12. Nakatsugawa I, Kamado S, Kojima Y, Ninomiya R, Kubota K (1998) *Corros Rev* 16:558
13. Yuan GY, Liu ZL, Wang QD (2002) *Mater Lett* 56:53
14. Das SK, Davis LA (1998) *Mater Sci Eng* 98:1
15. Lunder O, Lein JE, Aune TKr, Nisancioglu K (1989) *Corrosion* 45:741
16. Mathieu S, Rapin C, Hazan J, Steinmetz P (2002) *Corros Sci* 44:2737
17. Makar GL, Kruger J (1993) *Int Mater Rev* 38:138
18. Song GL, Atrens A, StJohn D, Wu X, Naim J (1997) *Corros Sci* 39:1981
19. Song G, Atrens A, Wu X, Zhang B (1998) *Corros Sci* 40:1769
20. Makar GL, Kruger J, Joshi A (1988) In: Paris HG, Hunt WH (eds) *Advances in magnesium alloys and composites*, TMS, 105
21. Boukamp BA (1988) In: *Equivalent circuit software*. The Netherlands University of Twente, p 6
22. Bonora PL, Andrei M, Eliezer A, Gutman EM (2002) *Corros Sci* 44:729
23. Udhayan R, Bhatt DP (1996) *J Power Sources* 63:103
24. Song GL, Atrens A, Dargush M (1999) *Corros Sci* 41:249
25. Qudong W, Yizheng L, Xiaoqing Z, Wenjiang D (2000) *Trans Nonferrous Met Soc China* 10:235